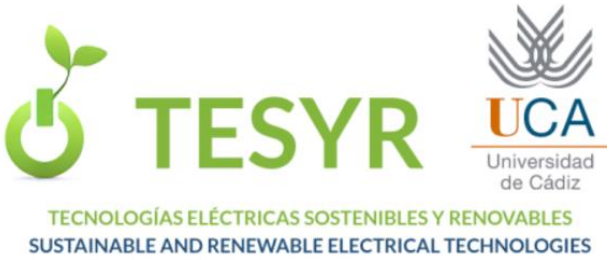

Universidad de Cádiz

Coordinated Operation of Multi-Energy Microgrids Based on Fuzzy-Logic Control

Pablo Horrillo-Quintero, Pablo García-Triviño, Ehsan Hosseini, Carlos Andrés García-Vázquez, Higinio Sánchez-Sainz and Luis M. Fernández-Ramírez

Published in:
24th International Conference on Environment and Electrical Engineering and 8th I&CPS Industrial and Commercial Power Systems Europe (EEEIC24)

DOI (link to publication from Publisher):
10.1109/EEEIC/ICPSEurope61470.2024.10751380

Publication date:
Not available

Document Version:
Accepted version

Citation for published version (IEEE):
P. Horrillo-Quintero, P. García-Triviño, Ehsan-Hosseini, C. Andrés García-Vázquez, H. Sánchez-Sainz and L. M. Fernández-Ramírez, "Coordinated Operation of Multi-Energy Microgrids Based on Fuzzy-Logic Control," *2024 IEEE International Conference on Environment and Electrical Engineering and 2024 IEEE Industrial and Commercial Power Systems Europe (EEEIC / I&CPS Europe)*, Rome, Italy, 2024, pp. 01-06, doi: 10.1109/EEEIC/ICPSEurope61470.2024.10751380.

Coordinated Operation of Multi-Energy Microgrids Based on Fuzzy-Logic Control

1st Pablo Horrillo-Quintero
SURET Research Group
Department of Electrical Engineering
University of Cadiz
Algeciras, Spain
pablo.horrillo@uca.es

2nd Pablo García-Triviño
SURET Research Group
Department of Electrical Engineering
University of Cadiz
Algeciras, Spain
pablo.garcia@uca.es

3rd Ehsan-Hosseini
SURET Research Group
Department of Electrical Engineering
University of Cadiz
Algeciras, Spain
ehsan.hosseini@uca.es

4th Carlos Andrés García-Vázquez
SURET Research Group
Department of Electrical Engineering
University of Cadiz
Algeciras, Spain
carlosandres.garcia@uca.es

5st Higinio Sánchez-Sainz
SURET Research Group
Department of Electrical Engineering
University of Cadiz
Puerto Real, Spain
higinio.sanchez@uca.es

6th Luis M. Fernández-Ramírez
SURET Research Group
Department of Electrical Engineering
University of Cadiz
Algeciras, Spain
luis.fernandez@uca.es

***Abstract*—The main approach on multi-energy microgrid (MEMG) study have been focused on optimization problems, without considering the dynamic control and real-time energy dispatch. This paper presents a new fuzzy-logic control method for a MEMG consisting of electricity, hydrogen, heating/cooling vectors. A PV power plant is the main renewable energy source selected. The thermal sources comprise an electric boiler and an absorption chiller, supplied by renewable energy. Furthermore, a gas boiler is considered to control the hot water thermal circuit. A hybrid energy storage system (ESS) is incorporated, encompassing a battery and a hydrogen system. The fuzzy-logic based energy management system (FL-EMS) is presented to dynamically perform a coordinated operation between the different energy vectors. Fuzzy logic algorithm is based on the PV energy and state-of-energy (SOE) of the ESS to dynamically assess the temperature control of the thermal sources. To assess the control efficacy and FL-EMS, a simulation lasting 4.5 hours was conducted under diverse operational conditions involving solar irradiance, heating, cooling, and electrical demand. The funding shows the efficacy of the FL-EMS in reducing dependency on the local grid, thus demonstrating the appropriateness of this approach for MEMGs.**

Keywords—multi-energy microgrid, dynamic control, fuzzy logic, power, hydrogen, heating, cooling.

I. Introduction

In the contemporary society, urban centers and industrial sectors have consistently escalated their requirements for electricity, gas heating, and cooling. Within the conventional energy paradigm, various energy systems are meticulously planned, designed, and operated autonomously, despite their intricate physical interconnections [1]. To enhance the energy utilization efficiency and accommodate the hosting capacity of renewable energy, there is a growing imperative for the interconnectedness and integration of diverse energy systems. The coordinated operation of several energy vectors is achieved through the implementation of multi-energy microgrids (MEMG) [2].

Research on MEMGs has traditionally focused on the static point of view, examining extended hourly or daily operational timeframes. This conventional modeling method concentrates its effort on the optimal energy dispatching, optimizing a cost function subjected to pre-established constraints [3]. Nevertheless, this approach in the study of MEMG does not include different dynamic processes with varying time scales for an interconnected electricity and thermal system. Thermal systems have a high inertia and are considerably slower than power systems.

Authors in [4] proposed an optimization algorithm to minimize the total operational cost of a MEMG comprising wind renewable production, energy storage systems (ESSs), combined heat and electricity units, and demand response programs. In [5], the optimization problem includes carbon emissions, underground water extraction, independency of the upstream grid and overall cost operation.

Intelligent algorithms are frequently employed to address optimization problems. For example, in [6], a multi-agent deep reinforcement learning was presented to enhance the power dispatching problem between several energy routers and the main grid in a decentralized approach, but it did not encompass the exploration of operating scenarios under extreme conditions. In [7], a stochastic-weighted optimization was analyzed for a building MEMG, considering practical thermal loads and battery degradation. However, the solutions provided may not be sufficient if the operating point deviates significantly from the point of linearization. Similar optimization inquiries were presented in [8], [9].

The aforementioned investigations underscore a void in dynamic modeling and control within the MEMG domain. The dynamic outlook introduces a novel exploration realm for the synchronized regulation of multiple interconnected energy vectors, seeking real-time and efficient energy dispatch. A notable consideration must be given to the operational parameters, encompassing ESS state of charge (SOC), meteorological scenarios, and the disparate temporal reactions of electrical and thermal dynamics. This consideration is imperative to enable an appropriate control response and expand the operational range beyond linearized models constrained to fixed parameters.

This paper strives to provide innovative methodologies for the dynamic examination and regulation of MEMGs, intending to assess real-time control. This study focuses on an intelligent dynamic fuzzy-logic EMS (FL-EMS) for a grid-connected MEMG composed of several energy vectors. The

This work was partially supported by Ministerio de Ciencia e Innovación, Agencia Estatal de Investigación, and Unión Europea (Grant TED2021-129631B-C32 supported by MCIN/AEI/10.13039/501100011033 and NextGenerationEU/PRTR).

979-8-3503-5518-5/24/$31.00 ©2024 IEEE

hot thermal sources encompass an electrical and gas boiler. An absorption chiller is included in the cooling network to meet the cooling requirements. A PV power plant is employed as the main renewable source to supply the MEMG. Furthermore, a hybrid ESS composed for a lithium-ion battery and a hydrogen system comprising an electrolyzer, a fuel cell and a hydrogen tank supports the renewable energy production.

The remaining sections of this manuscript are structured as follows: Section II describes the configuration of the MEMG, and Section III explains the fuzzy-logic-based EMS and control scheme. Section IV presents and discusses the results and finally, Section V outlines the conclusions drawn from this research.

II. Multi-Energy Microgrid Configuration

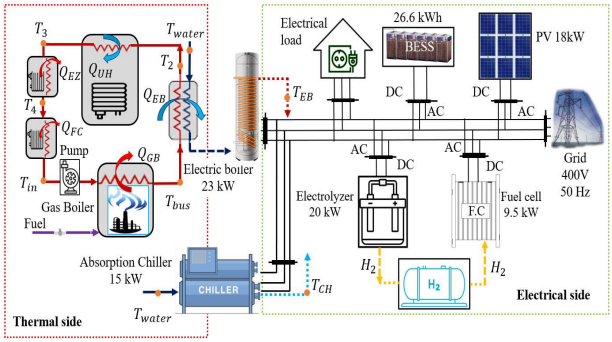

Fig.1 Schematic configuration of the proposed MEMG.

A schematic configuration of the MEMG is shown in Fig. 1. The thermal carrier is split into two independent hot water and cooling water circuits. A 23-kW electric boiler supplied by renewable energy fulfils the hot water demand, whereas a gas boiler regulates the temperature of the hot thermal bus and supports the electric boiler. The thermal load is represented through an underfloor heating domestic demand, connected to the hot water circuit. Moreover, a 15-kW absorption chiller is connected to the cooling water circuit to satisfy the cooling demand.

The electricity carrier of the MEMG incorporates a PV power plant with a peak capacity of 18 kWp, comprising six strings of ten modules of 300 W, an electrical load and a three-phase local grid of 400V. The hybrid ESS is based on a 26.6 kWh lithium-ion battery and a green hydrogen system. It consists of a 9.5 kW fuel cell, a 20 kW electrolyzer and a 1 kg hydrogen tank. Table I collects the electrical and thermal parameters.

A. Thermal Vector Modeling

The thermal components are designed employing the *CARNOT toolbox* within MATLAB/Simulink, a tool created by the Institute of Solar Research in Juelich, Germany [10]. The gas boiler output temperature can be dynamically modelled based on the energy balance and the first thermodynamic law [11,12]:

$$\left(m \cdot c \cdot \frac{1}{N}\right) \cdot \frac{dT_{bus}}{dt} = \left(U \cdot A \cdot \frac{1}{N}\right) \cdot (T_{amb} - T_{bus}) + (\dot{m}_{bus} \cdot c_f) \cdot (T_{in} - T_{bus}) + Q_{GB} \quad (1)$$

$$C_{EB} \cdot \frac{dT_{EB}}{dt} = U \cdot A \cdot (T_{amb} - T_{EB}) + (\dot{m}_{water} \cdot c_p) \cdot (T_{bus} - T_{EB}) + P_{EB} \quad (2)$$

In a similar perspective, the electric boiler is modelled as an electric heater powered by renewable energy, according the energy balance and the thermal losses to the ambient [11,12].

The absorption chiller relies on the characteristic curves and the coefficient of performance of a real chiller unit. These curves are derived from the reversible air-to-water heat pump with waste heat recovery LI 16TER+ model provided by Dimplex [13].

B. Electricity Vector Modeling

The selection of the PV system arrangement outlined in [14] is based on its proven accuracy and straightforward design, as supported by prior investigations [15].

The battery model, derived from the *SimPowerSystems Toolbox* embedded in Simulink [16], has been selected. It has been designed across the Voltage-Current (V-I) and Voltage-SOC (V-SOC) datasheet curves, as well as the dynamic response of the battery. The SOC is formulated by Equation (3).

$$\mathrm{SOC}(\%) = \mathrm{SOC_0}(\%) - 100\left(\frac{\int I_{BESS} \cdot dt}{E_{BESS}^{rated}}\right) \quad (3)$$

C. Hydrogen Vector Modeling

The electrolysis model utilized in this investigation is founded on the proton exchange membrane (PEM) model documented in the *Simscape library* [17]. The PEM electrolyzer employs renewable energy to perform the electrolytic separation of water into hydrogen and oxygen. Additionally, it accounts for the thermal energy released during the electrolysis procedure.

The fuel cell model is selected from the PEM fuel cell model documented in [18] within the *Simscape library*. The PEM fuel cell generates electric power by consuming the green hydrogen produced during the electrolysis. Sustaining the ideal temperature and humidity levels in the fuel cell stack is imperative for effective functioning across diverse loads. Consequently, the thermal energy produced during

TABLE I. Electrical and Thermodynamic Parameters.

Symbol	Parameter	Unit
C_{EB}	Thermal capacity of the boiler	J/K
c	Heat capacity boiler	J/(kg·K)
c_f, c_p	Heat capacity of fluid	J/(kg·K)
E_{BESS}^{rated}	BESS rated capacity	Wh
m	Mass of the boiler	kg
$\dot{m}_{bus}, \dot{m}_{water}$	Bus water and local network mass flow rate	Kg/s
N	Number of nodes	-
P_{EB}	Electric boiler power	W
I_{BESS}	BESS current	A
$P_{BESS,char-dis}^{max}$	Maximum BESS power in charging/discharging mode	W
Q_{EB}	Heat power of the boiler	W
T_{amb}	Ambient temperature	ºC
T_{bus} , T_{EB}, T_{CH}	Hot water bus, electric boiler and chiller temperature	ºC
T_{in}	Temperature of fluid at the input	ºC
UA	Heat loss coefficient to ambient	W/K

electrolysis is reclaimed and recirculated within the hot water circuit.

III. Fuzzy-Logic EMS and Control Loops

As mentioned above, this paper proposes a FL-EMS to perform the dynamic supervisory control of the MEMG presented in Section II. The aim of this FL-EMS is to establish an efficient coordination of the electricity, heating, cooling and hydrogen vectors while ensuring the electrical and thermal demands. It is noteworthy that the controlled components in the MEMG are thermal sources and the ESSs, as energy support for the renewable energy production. Thus, the PV power plant operates at the maximum power point (MPPT) according to a Perturbe&Observe (P&O) algorithm and is not considered in the fuzzy logic inference.

A. Fuzzy Logic Energy Management System

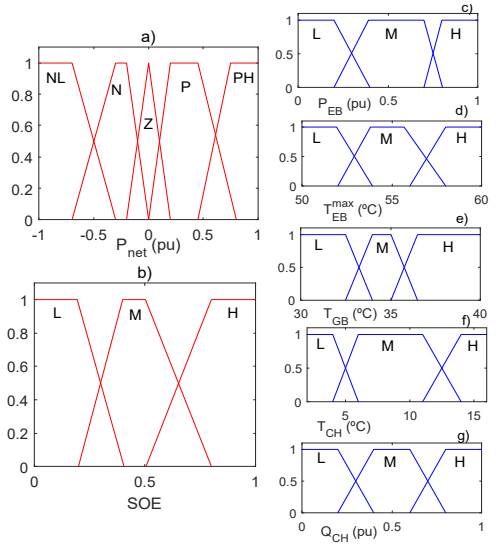

Fig. 2. Membership functions: a) Renewable energy available (P'_{NET}), b) ESS SOE, c) electric boiler power (P_{EB}), d) electric boiler turn-off temperature (T^{EB}_{max}), e) temperature in the thermal bus (T_{bus}), f) absorption chiller turn-off temperature (T^{EB}_{max}), and g) absorption chiller cooling production (Q_{CH}).

The novelty of the presented FL-EMS lies in dynamically establishing the operating point of the thermal sources, taking into account the renewable power available (P'_{NET}) and the state-of-energy (SOE) of the ESSs. P'_{NET} is the difference between the PV production (P_{PV}) and the electrical load (P_{LOAD}). On the other hand, the *SOE* of the ESS allows us to illustrate the BESS SOC and the hydrogen level (H_L) in a unique parameter, which is defined as follows [19]:

$$SOE = (E^{dis}_{H2} + E^{dis}_{BESS})/(E^{rated}_{H2} + E^{rated}_{BESS}) \quad (4)$$

where, E^{dis}_{H2} is the energy disponible in the hydrogen tank, E^{dis}_{BESS} is the energy disponible in the battery, E^{rated}_{H2} is the rated energy in the hydrogen tank, and E^{rated}_{BESS} represents the battery rated capacity. These parameters are defined in detail in [19].

Five outputs are considered in the FL-EMS: the reference temperature for the hot thermal bus (T^{ref}_{bus}), the maximum temperature of the electric boiler (T^{max}_{EB}), the electric boiler consumption (P_{EB}), the maximum temperature of the absorption chiller (T^{max}_{CH}), and the cooling energy supplied by the chiller (Q_{CH}). Concerning the membership functions (MFs), five are utilized to characterize P'_{NET} (NL, N, Z, P, PH), and three for SOE, $P_{EB}, T^{ref}_{bus}, T^{max}_{EB}$, T^{max}_{CH} and Q_{CH} (L,M,H), as depicted in Figure 2. The system behavior is delineated by 25 rules (Table II), utilizing a Mamdani-type inference approach.

TABLE II. Rule Base for the Fuzzy Logic System.

INPUTS		OUTPUTS				
P'_{NET}	SOE	P_{EB}	T^{max}_{EB}	T^{ref}_{bus}	T^{max}_{CH}	Q_{CH}
NL	L	L	L	H	H	L
NL	M	L	M	H	M	L
NL	H	M	M	H	M	M
N	L	L	L	M	H	L
N	M	L	M	M	M	L
N	H	M	H	M	L	M
Z	L	L	M	M	M	L
Z	M	M	M	M	M	M
Z	H	H	M	M	L	H
P	L	M	M	H	M	M
P	M	H	M	H	L	H
P	H	H	H	L	L	H
PH	L	H	M	L	M	H
PH	N	H	H	L	L	H
PH	H	H	H	L	L	H

The goal of the FL-EMS is to minimize the reliance on the local grid to supply the thermal and electrical loads. Therefore, if P'_{NET} takes a high value, that means that the renewable energy acts as the main energy carrier. The electric boiler is able to operate in high temperatures, while the absorption chiller works in low temperatures, and the gas consumption is reduced to maintain the temperature in the hot thermal circuit. On the other hand, if P'_{NET} takes a low value, that means that there is insufficient renewable energy to supply the thermal sources. T^{max}_{EB} is reduced, whereas T^{max}_{CH} is incremented to reduce the power consumption. The gas boiler rises T^{ref}_{bus} to compensate the reduction in T^{max}_{EB} and to maintain the comfort in the hot water demand.

This operating mode enables a more intelligent energy use and lower consumption. This is because FL avoids an all-or-nothing consumption, regulating in each moment the consumption of the electric boiler and the absorption chiller, and it is not fixed to their rated power. Considering the SOE of the ESSs, FL assesses fluctuations in the PV energy production and avoids the consumption of the local grid, providing a wide operating range, as multiple conditions are

considered simultaneously to provide a proper control response.

FL computes, for each operating condition, the functional point of thermal sources and ESSs, applying the rules established in Table II. This enables the optimization of energy distribution, unlike simple techniques based on EMS that assign similar operating points within predefined operating ranges. Another noteworthy innovation is the proposed structure for the FL, where only two parameters (P'_{NET} and SOE) are required to calculate the operating point of the MEMG.

B. Control Loops

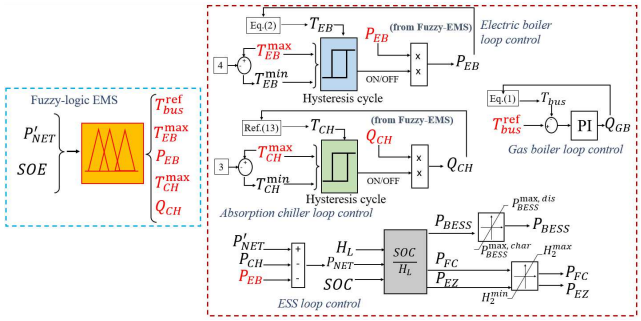

Fig.3 Overall MEMG control scheme.

The overall control loop scheme implemented to regulate the thermal sources and the ESSs according to the FL-EMS references is shown in Fig. 3. The control loops are divided into four independent control loops. The electric boiler loop control is based on a hysteresis cycle. The turn-off temperature of the electric boiler (T_{EB}^{max}) and the electric power consumption (P_{EB}) are provided by the FL-EMS, while the turn-on temperature (T_{EB}^{min}) is calculated as 4ºC lower than T_{EB}^{max}. Thereby, the electric boiler constantly adapts its operating mode, and a fast control response is achieved under changes in weather conditions and electrical demand.

Similarly, the absorption chiller loop control is designed using a hysteresis cycle. The aim of adopting a hysteresis control cycle is to avoid supplying constant energy to the chiller as well to the electric boiler. Thus, it is possible to save energy when the hysteresis cycle increases (for the absorption chiller cooling system) and when it decreases (for the electric boiler heating system). The turn-on temperature of the chiller (T_{CH}^{max}) and the cooling heat (Q_{CH}) are provided by the FL-EMS, while the turn-off temperature (T_{CH}^{min}) is calculated as 3ºC lower than T_{CH}^{max}.

The gas boiler control loop is responsible for regulating the hot water thermal bus. Owing to the heating and hot water demands, the temperature drops in the hot water bus (T_{bus}). Therefore, a PI controller is employed to regulate T_{bus} according to the reference sent by the FL-EMS (T_{bus}^{ref}).

The ESS control loop is responsible for distributing energy between the battery and the hydrogen system, and minimizes the reliance on the main grid. The energy that the ESSs must manage is calculated as the difference between P'_{NET} and the consumption of the thermal sources, according to Equation (5):

$$P_{NET} = P'_{NET} - P_{EB} - P_{CH} \tag{5}$$

where P_{CH} is the electrical consumption of the absorption chiller, which is obtained through the cooling demand (Q_{CH}) and the coefficient-of-performance (COP) included in [13].

A proportional sharing factor, denoted as SOC/H_L, where H_L denotes the hydrogen tank level, is established to distribute the energy between the ESSs. This parameter denotes that when SOC>H_L, the BESS energy is higher than the fuel cell energy in the discharging mode. Conversely, when the ESSs operates in the charging mode, the electrolyzer obtains a greater amount of power than the BESS. If $SOC<H_L$, then the power distribution between the ESSs is reciprocally related to the previously detailed scenario.

This study presents a dynamic constraint based on the SOC to prolong the operational lifespan of the BESS. The upper limit for discharging, denoted as $P_{BESS,dis}^{max}$, or charging, denoted as $P_{BESS,char}^{max}$, is restricted in accordance with the subsequent equations:

$$P_{BESS,dis}^{max} = min\left(P_{BESS}^{rated}, \frac{E_{BESS}^{nom}}{\Delta t} \cdot \left(\frac{SOC - SOC_{min}}{100}\right)\right) \tag{6}$$

$$P_{BESS,ch}^{max} = min\left(P_{BESS}^{rated}, \frac{E_{BESS}^{nom}}{\Delta t} \cdot \left(\frac{SOC_{max} - SOC}{100}\right)\right) \tag{7}$$

The dynamic limitations established in Eqs. (6) and (7), delineate P_{BESS}^{max}, delivering the maximum power capability of the BESS at each moment. P_{BESS}^{rated} corresponds to the rated power of the BESS and complies with the SOC restrictions, preserving the SOC within predetermined upper and lower thresholds (SOC_{max}, SOC_{min}). These thresholds are set at 90% and 30%, respectively, avoiding a deep discharge. Additionally, the hydrogen tank level is constrained within 10% and 100% of its rated capacity.

IV. Results and Discussion

This section analyses the designed FL-EMS and the control scheme for the MEMG presented in Section II. The model is developed in MATLAB/Simulink. In the majority of studies that address MEMGs research, the optimization problem is evaluated under long hourly or daily time horizons. Because of the faster electricity dynamic compared with the thermal one, this paper presents a 4.5 h simulation to assess the control approach of the MEMG and ensure a proper response of the thermal and electricity vectors.

The MEMG control is verified by varying the inputs parameters, which are shown in Fig. 4. It is represented the hot water demand profile in Fig. 4a (m_H), the cooling water demand profile in Fig. 4b (m_C), the underfloor heating load in Fig. 4c (m_{UH}), and the PV power plant irradiance in Fig. 4d (I).

The electricity vector balance is illustrated in Fig. 5. As mentioned in Section III, the electricity vector energy distribution is designed to fulfil the electrical load as well as the electric consumption of the thermal sources without employing the local grid. Fig. 4a shows with positive values the energy supplied by the MEMG while the energy consumed by the MEMG is illustrated with negative values.

In this study case, it is shown the evolution of P_{PV} from high values, in the beginning of the simulation (18kW), to low values at the end of the simulation (1.6kW). In the initial

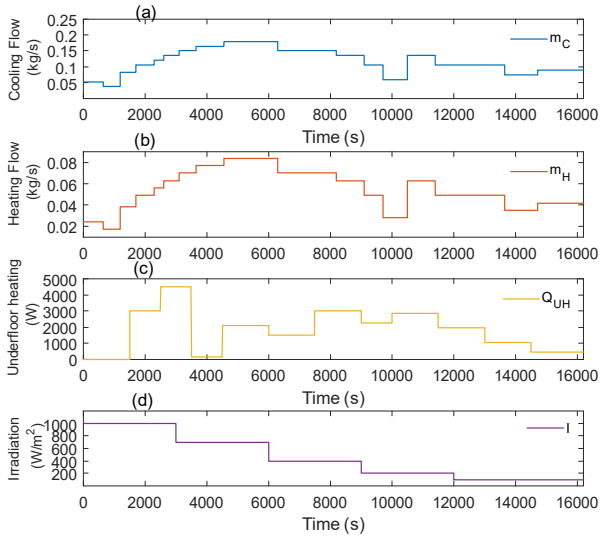

Fig. 4. (a) Cooling water mass flow demand (m_C), (b) Hot water mass flow demand (m_H), (c) thermal underfloor heating demand (Q_{IIH}), and

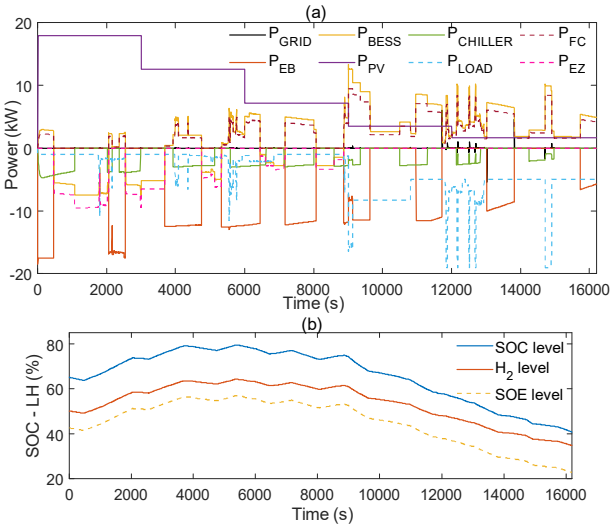

Fig. 5. (a) Electric power balance for the MEMG, and (b) SOC of the BESS hydrogen level (H_L) and state-of-energy (SOE).

conditions, the electric boiler consumes -17.5 kW and the ESSs are discharged to fulfill the chiller and the electric load demand. As seen, the battery provides more energy than the fuel cell because SOC>H_L. When the electric boiler is off, the ESSs change their operation mode and the electrolyzer receives more energy than the battery. From 4000s to 9500s, the PV power plant experiments several energy reductions, and the electric boiler adapts its consumption to -12.5 kW and the ESSs are deeply discharged. From 12000s, unseasonable electrical loads are considered to taste the fast response of the ESSs and avoid the consumption of the local grid. As seen, no energy is provided by the grid even in this extreme scenario.

The evolution of the SOC, H_L and SOE levels are shown in Fig. 5b. These parameters evolve according to the proportional energy distribution in the charging and discharging modes, limiting the BESS discharge energy and hydrogen consumed by the fuel cell when they are near 30% and 10%, respectively.

The thermal vector balance is depicted in Fig. 6. To satisfy the thermal balance, the thermal energy generated (Q_{GEN})

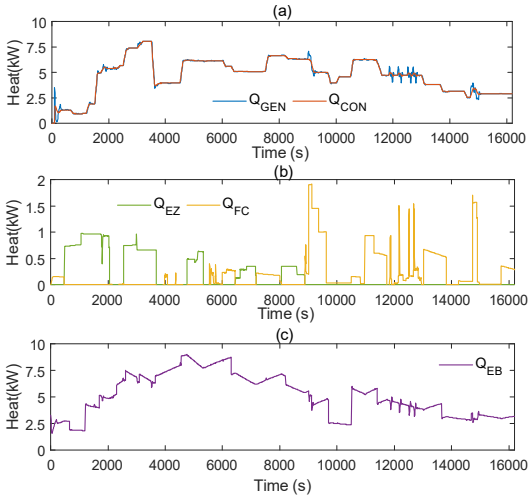

Fig. 6. (a) Thermal power generated (Q_{GEN}) and thermal power consumed (Q_{CON}) , (b) thermal power injected by the electrolyzer (Q_{EZ}) and thermal power injected by the fuel cell (Q_{FC}), and (c) thermal power supplied by the electric boiler (Q_{EB}),

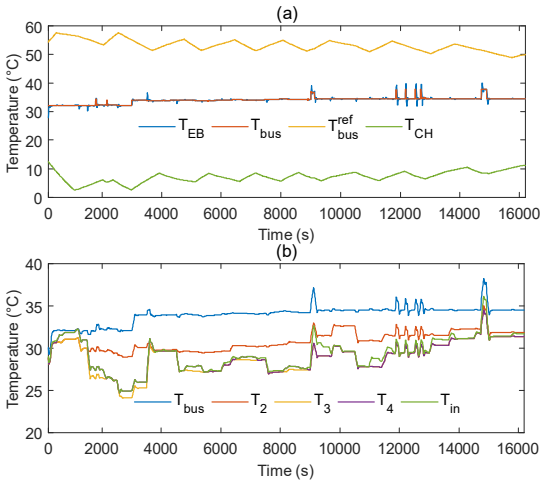

Fig. 7. (a) Thermal bus temperature (T_{bus}), reference temperature of thermal bus (T_{bus}^{ref}) , electric boiler temperature (T_{EB}), and absorption chiller temperature (T_{CH}), and (b) Nodes temperatures: Bus temperature (T_{bus}), electric boiler output (T_2), underfloor heating output (T_3), electrolyzer output temperature (T_4) and fuel cell output temperature (T_{in}).

must be equal than the heat consumed (Q_{CON}). Fig. 6a represents the proper control response achieved.

During the electrolysis process, the heat generated can be recovered and injected into the hot water thermal circuit. This allows for the reduction of gas consumption. Fig. 6b shows the heat generated by the fuel cell (Q_{FC}) and the heat generated by the electrolyzer (Q_{EZ}). The total heat energy generated, (E_{GEN}) is calculated as the integral time of Q_{GEN}. It takes a value of 21,17 kWh. The heat energy recovered in the fuel cell (E_{FC}) is 0.87 kWh (4.1% of the total) and in the case of the heat energy recovered in the electrolyzer(E_{EZ}) is 0.94 kWh (4.4% of the total). Therefore, a total amount of 8.5% of the energy is saved by employing the heat produced in the electrolysis process.

Finally, the temperature control of the thermal sources is illustrated in Fig. 7a. As described in Section III, the electric boiler and the absorption chiller are controlled through a

hysteresis cycle, while the hot water bus temperature is controlled employing a PI controller. This efficient temperature control enables to rise T_{EB}^{max} while decreasing T_{bus} if there is a surplus of renewable energy. On the other hand, T_{EB}^{max} is reduced if the PV power production is low and elevates T_{bus} to mitigate this scenario.

The use of FL permits to discretize the temperature control, and avoids a control based on low, medium or high temperatures, where multiple operating conditions can be considered and dynamically adjusted. For instance, at the beginning of the simulation, T_{EB}^{max} is set at 57.5ºC, as P_{PV} is high (18 kW), and SOE has an intermediate value (40%). The gas boiler is controlled at 32 °C, and the absorption chiller can operate at a low temperature (2.5ºC). When P_{PV} curtails is energy from 4000s to 9500s, the chiller increments its turn-on temperature at the same time as the electric boiler decreases its turn-off temperature to mitigate the energy consumption. In this scenario, the gas boiler needs to increment T_{bus} to maintain the heat balance. Finally, when the SOE assesses a low value in the last instances of the simulation (from 14000s), and P_{PV} is set at 1.6kW, it is seen in Fig. 7a the decreasing trend in the hysteresis cycle of the electric boiler in addition to the increasing trend of the absorption chiller.

The temperature falls in the hot water demand because of the hot water consumption and rises owing to the heat recovered from the electrolysis process in the fuel cell and the electrolyzer. The temperature drops are shown in Fig. 7b. The node temperature after the electric boiler heat exchanger is denoted as T_2, in the underfloor heating demand output as T_3, in the electrolyzer heat exchange output as T_4 and as T_{in} after the fuel cell heat exchange. For example, it is represented in Fig. 7b at 3000s, that when the electrolyzer is operating, $T_4 > T_3$, and thereby, less fuel is consumed by the gas boiler. Analogously, at 11000s, when the fuel cell is turned on, $T_{in} > T_4$ and fuel is saved.

V. Conclusions

The aim of this paper was to present a control architecture for a MEMG that avoid the consumption of the local grid to supply the thermal and electrical loads. The innovation lay in dynamically regulating the operating mode of the thermal sources in a sampling time of 0.02s, along with determining the energy to be overseen by the ESSs. The state of energy of the ESSs and the available renewable energy were the two parameters needed to achieve a proper coordinated operation between the different energy vectors. Furthermore, dynamic constraints were established for the ESSs to adapt their energy contribution. The heat produced in the electrolysis process for the fuel cell and the electrolyzer could be used in the hot water demand to reduce the gas consumption. An 8.5% saving in the gas consumption was achieved in the proposed scenario. The control strategy was evaluated in a 4.5h simulation under several weather conditions and both thermal and electrical loads, and a proper control response was achieved. Future works should include the experimental real-time validation of the proposed FL-EMS.

References

[1] "State Estimation for Integrated Energy Systems: Motivations, Advances, and Challenges PREPARED BY THE IEEE PES Energy Internet Coordinating Committee IEEE PES Working Group on Power System Static and Dynamic State Estimation Task Force on State Estimation for Integrated Energy Systems IEEE Power & Energy Society PES-TR118," 2023.

[2] P. Ye, K. Qu, F. Sun, M. Zhang, and N. Zhang, "Research status and Prospect of integrated energy system collaborative control based on energy Internet," in E3S Web of Conferences, EDP Sciences, May 2021.

[3] L. Tan, P. Wang, W. Wang, and D. Xu, "Optimal Operation of Multi-energy Complementary Microgrid with Cooling, Thermal and Electricity Load," in 2021 3rd AEEES 2021, Institute of Electrical and Electronics Engineers Inc., Mar. 2021, pp. 599–604.

[4] Q. Y. Wang, X. L. Lv, and A. Zeman, "Optimization of a multi-energy microgrid in the presence of energy storage and conversion devices by using an improved gray wolf algorithm," Appl Therm Eng, vol. 234, Nov. 2023,

[5] Q. Y. Wang, X. L. Lv, and A. Zeman, "Optimization of a multi-energy microgrid in the presence of energy storage and conversion devices by using an improved gray wolf algorithm," Appl Therm Eng, vol. 234, Nov. 2023,

[6] B. Zhang, W. Hu, A. M.Y.M. Ghias, X. Xu, and Z. Chen, "Multi-agent deep reinforcement learning based distributed control architecture for interconnected multi-energy microgrid energy management and optimization," Energy Convers Manag, vol. 277, Feb. 2023,

[7] Z. Li, L. Wu, Y. Xu, and X. Zheng, "Stochastic-Weighted Robust Optimization Based Bilayer Operation of a Multi-Energy Building Microgrid Considering Practical Thermal Loads and Battery Degradation," IEEE Trans Sustain Energy, vol. 13, no. 2, pp. 668–682,

[8] A. Mobasseri, M. Tostado-Véliz, A. A. Ghadimi, M. Reza Miveh, and F. Jurado, "Multi-energy microgrid optimal operation with integrated power to gas technology considering uncertainties," J Clean Prod, vol. 333, Jan. 2022,

[9] H. Masrur, H. Khaloie, A. T. Al-Awami, S. El Ferik, and T. Senjyu, "Cost-aware modeling and operation of interconnected multi-energy microgrids considering environmental and resilience impact," Appl Energy, vol. 356, Feb. 2024,.

[10] Solar Institut Jülich, CARNOT – Conventional And Renewable eNergy CARNOT – Conventional And Renewable Energy Systems OptimizationToolbox.

[11] S. Lohmann, "Einführung in die Software MATLAB® - Simulink® und die Toolboxen CARNOT und Stateflow® zur Simulation von Gebäude- und Heizungstechnik,"

[12] G. Salvadori, L. Ferrari, L. Romano and F. Fantozzi, "Use of CARNOT Toolbox to Evaluate the Impact of Building Automation and Control Systems on Energy and CO2 Emission Savings," (EEEIC / I&CPS Europe), Madrid, Spain, 2020, pp. 1-6, doi: 10.1109/EEEIC/ICPSEurope49358.2020.9160742.

[13] P. Heizen and K. mit Dimplex Wärmepumpen, "PHB_WP_Heizen_Kuehlen_ES." [Online]. Available: www.dimplex.de

[14] W. De Soto, S. A. Klein, and W. A. Beckman, "Improvement and validation of a model for photovoltaic array performance," Sol Energy 2006;80(1):78–88.

[15] M. G. Villalva, J. R. Gazoli, and E. R. Filho, "Comprehensive approach to modeling and simulation of photovoltaic arrays," IEEE Trans Power Electron 2009;24(5): 1198–208.

[16] SimPowerSystems TM. Reference. Natick, MA: Hydro-Quebec and the MathWorks. Inc; 2015.

[17] The MathWorks, Inc. "PEM Electrolysis System" mathworks.com. Accessed: January 03, 2024. [Online]. Available: https://www.mathworks.com/help/stats/index.html.

[18] The MathWorks, Inc. "PEM Fuell System" mathworks.com. Accessed: January 03, 2024. [Online]. Available: https://es.mathworks.com/help/simscape/ug/pem-fuel-cell-system.html?lang=en.

[19] P. Garcia-Trivino, L. De Oliveira-Assis, E. P. P. Soares-Ramos, R. Sarrias-Mena, C. A. Garcia-Vazquez, and L. M. Fernandez-Ramirez, "Supervisory Control System for a Grid-Connected MVDC Microgrid Based on Z-Source Converters With PV, Battery Storage, Green Hydrogen System and Charging Station of Electric Vehicles," IEEE Trans Ind Appl, vol. 59, no. 2, pp. 2650–2660, Mar. 2023,